Thermal, Physical, and Electrochemical Properties of $Li[N(SO_2F)_2]$-[1-ethyl-3-methylimidazolium][$N(SO_2F)_2$] Ionic Liquid Electrolytes for Li Secondary Batteries Operated at Room and Intermediate Temperatures

Kazuhiko Matsumoto[a,*], *Erisa Nishiwaki*[a], *Takafumi Hosokawa*[a], *Shinya Tawa*[a], *Toshiyuki Nohira*[b], *Rika Hagiwara*[a]

[a]Graduate School of Energy Science, Kyoto University, Yoshida, Sakyo-ku, Kyoto 606–8501, Japan

[a]Institute of Advanced Energy, Kyoto University, Gokasho, Uji 611-0011, Japan

Phone: +81 75 753 5822, Fax: +81 75 753 5906,

E–mail: k-matsumoto@energy.kyoto-u.ac.jp (Kazuhiko Matsumoto)

Abstract

The Li[FSA]-[C_2C_1im][FSA] (FSA^-: bis(fluorosulfonyl)amide and $C_2C_1im^+$: 1-ethyl-3-methylimidazolium) ionic liquids have been studied as electrolytes for Li secondary batteries, though their thermal, physical, and electrochemical properties have not been systematically characterized. In this study, the thermal and transport properties of Li[FSA]-[C_2C_1im][FSA] ionic liquids as a function of the Li[FSA] molar fraction and temperature, in view of their operation at both room and intermediate temperatures. Differential scanning calorimetric analysis revealed that this system has a wide liquid-phase temperature range from Li[FSA] fractions of 0.0 to 0.4 and indicated the existence of the Li[C_2C_1im][$FSA]_2$ line compound. Single-crystal X-ray diffraction analysis was used to determine the crystal structure of Li[C_2C_1im][$FSA]_2$, which consists of Li^+ octahedrally coordinated by six O atoms originating from four FSA^- anions. The temperature dependences of the viscosity and ionic conductivity were fitted by the Vogel–Tammann–Fulcher equation, and the viscosity and molar ionic conductivity were connected by the fractional Walden rule. Lithium-metal deposition/dissolution efficiency decreased with increasing measurement temperature and decreasing Li[FSA] fraction. Aluminium corrosion at positive potentials was investigated by a potential step method, which revealed that the stability of an aluminium electrode was improved at high Li[FSA] fractions at 298 K and the corrosion-limit potential decreased at elevated temperatures.

.

Introduction

Recently, there have been remarkable developments in energy-storage technology all over the world with Li secondary batteries being one of the most widely used energy-storage devices under various circumstances owing to their high power and energy densities.[1-3] Ionic liquids, which exclusively consist of ions and, therefore, possess intrinsic ionic conductivity, are considered to be alternative non-aqueous electrolytes for various energy-storage devices.[4-7] Their unique properties such as low volatility, low flammability, and a wide liquid-phase temperature range enable the construction of reliable high-power and high-energy devices.[8-10]

Both bis(trifluoromethylsulfonyl)amide ($TFSA^-$) and bis(fluorosulfonyl)amide (FSA^-) anions have been used in electrochemical applications, with FSA^- now widely used as a counteranion for designing ionic-liquid electrolytes.[11] Most ionic liquids have high viscosities that are more than an order of magnitude greater than those of popular organic electrolytes. However, FSA^--based ionic liquids tend to exhibit relatively low viscosities (e.g. 18 mPa s for $[C_2C_1im][FSA]$ ($C_2C_1im^+$ = 1-ethyl-3-methylimidazolium) at 298 K) and, thus, high ionic conductivities (e.g. 15.4 mS cm^{-1} for $[C_2C_1im][FSA]$ at 298 K).[12] Furthermore, stable alkali-metal deposition/dissolution and Li^+ intercalation/deintercalation into/from graphite are possible in FSA^--containing ionic liquids without any additives, which makes them attractive electrolytes for secondary batteries.[12-18] A recent report attributed this high stability against reduction to the unusually low reactivity of the $\cdot SO_2NX^-$ radical anion intermediate.[19] Consequently, the electrochemical behavior of a number of electrode materials including graphite, Si, $LiCoO_2$, $LiFePO_4$, and $LiMn_{1/3}Co_{1/3}Ni_{1/3}O_2$ has been examined in FSA^--based or FSA^--$TFSA^-$-mixed ionic liquids in view of their potential application in Li secondary batteries.[20-33]

Understanding the basic thermal, physical, and electrochemical properties of ionic liquids is important for selecting an appropriate ionic liquid electrolyte for specific applications. The thermal and physical properties of FSA^- single salts and binary mixture of FSA^- salts containing Li^+ have been investigated previously. Most FSA^- single salts with organic cations exhibit low melting points compared to the corresponding salts with popular anions for ionic liquids.[12, 15, 28, 34-35] *N*-alkyl-*N*-

methylpyrrolidinium FSA salts either in the form of FSA^- salts or of FSA^--$TFSA^-$ mixed salts, are the most intensively studied in this series of ionic liquid electrolytes for Li secondary batteries.[17-18, 36-38] The Li[FSA]-[C_3C_1pyrr][FSA] ($C_3C_1pyrr^+$ = *N*-methyl-*N*-propylpyrrolidinium) binary system exhibits a wide liquid-phase temperature range and acceptable ionic conductivity.[37] Extension of the alkyl chain to $C_4C_1pyrr^+$ ($C_4C_1pyrr^+$ = *N*-butyl-*N*-methylpyrrolidinium) results in disappearance of the crystallization peak at high Li[FSA] concentrations and decrease of the liquidus temperature, though an increase in viscosity is also inevitable. Compared to the FSA system, the TFSA analogues, e.g. Li[TFSA]-[C_3C_1pyrr][TFSA] and Li[TFSA]-[C_4C_1pyrr][TFSA], crystallize more easily and have lower ionic conductivities.[12, 28, 39-40] Some line compounds have been detected crystallographically at specific ratios in such systems. For example, in the crystal structures of $Li_2[C_4C_1pyrr][TFSA]_3$ and $Li_2[C_3C_1pyrr][TFSA]_3$, which are isostructural with each other, Li^+ is coordinated by four or five $TFSA^-$ O atoms, including two bidentate $TFSA^-$ anions in the case of the five-coordination structure.[40]

Although the electrochemical stability of imidazolium-based ionic liquids is lower than that of pyrrolidinium-based ionic liquids when using the $TFSA^-$ anion, which prevents their use in practical batteries, the presence of FSA^- in these ionic liquids improves their electrochemical stability, as stated above. The high ionic conductivities of imidazolium-based ionic liquids are highly beneficial for high-rate charging and discharging. However, there has been no systematic characterization of the Li[FSA]-[C_2C_1im][FSA] binary system in terms of its thermal and transport properties as a function of the Li[FSA] fraction (*x*(Li[FSA]). Thus, we report here the detailed phase behavior and physical properties of this system. The ion-ion interactions and packing mode of the 1:1 salt (Li[C_2C_1im][$FSA]_2$) are also discussed based on its X-ray crystal structure. Electrochemical Li deposition/dissolution and Al corrosion behavior in this ionic liquid were examined by cyclic-voltammetric and potential-step methods. The corrosion of Al metal current collectors sometimes causes significant problems during cell operation, especially in electrolytes with sulfonylamide salts, and understanding the concentration and temperature dependence of this process is important from a practical perspective.[41] One of the important targets related to this study is the intermediate-temperature operation of Li secondary batteries. Our

previous works on Li and Na secondary batteries demonstrated several benefits of intermediate-temperature operation (298−423 K), such as operation under hot environments and the use of waste heat.[42-44] For such applications, investigating the temperature dependence of the physical and electrochemical properties of ionic liquid electrolytes is vitally important.

Experimental section

General experimental procedure. All non-volatile materials were handled in a drybox under an atmosphere of dry Ar. The ionic liquid $[C_2C_1im][FSA]$ (Kanto Chemical Inc., water content < 20 ppm) and Li[FSA] (Kishida Chemicals Co., Ltd., water content < 20 ppm) salts were dried under vacuum at 353 K.

Analysis. Differential scanning calorimetry (DSC) was performed using a DSC-8230 Thermo Plus EVO II Series (Rigaku Corp.) at a scan rate of 5 K min^{-1}. The samples for DSC were sealed in an airtight Al cell under an atmosphere of dry Ar. The viscosities of the ionic liquids were measured using a DV2T cone and plate rheometer (Brookfield Engineering Laboratories) under an atmosphere of dry air. Ionic conductivities were measured using AC impedance with a 3532-80 impedance analyzer (Hioki E.E. Corp.). The samples for the ionic conductivity measurements were sealed in an airtight T-shaped cell equipped with stainless-steel disk electrodes under an atmosphere of dry Ar. The cell was set in an SU-241 thermostatic chamber (ESPEC Corp.). Densities were measured using a DMA 4500M oscillating U-tube density meter (Anton Paar GmbH). Water contents were measured using the Karl-Fischer titration method (899 Coulometer, Metrohm). The surface of anodically polarized Al electrodes was analyzed by SU-8020 field-emission scanning electron microscopy (FE-SEM) and energy dispersion X-ray (EDX) spectrometry (Hitachi High-Technologies). The FE-SEM and EDX samples were washed with tetrahydrofuran in a drybox after electrochemical measurements and transferred into the vacuum chamber without exposure to the air.

Electrochemical measurements were performed using a VSP-300 system (BioLogic). The electrochemical window was tested by cyclic voltammetry measurements in a three-electrode system

with Cu disk, glass like carbon disk, and Al plate working electrodes. The reference and counter electrodes were Li metal immersed in the ionic liquid. The Li deposition/dissolution cycle efficiency (ε_{cycle}) was evaluated in a two-electrode cell at a current density of 1.0 cm^{-2} using a Hokuto Denko HJ1001SD8 system. Lithium metal of 1.0 C cm^{-2} was first deposited on a Cu substrate and Li dissolution and deposition of 0.2 C cm^{-2} was repeated until the electrode potential reached 0.5 V vs. Li^+/Li during the dissolution. The ε_{cycle} value was calculated according to Eq. (1):

$$\varepsilon_{cycle} = \frac{N_{eff} \cdot Q_{cycle}}{Q_{ex} + N_{eff} \cdot Q_{cycle}} \qquad \text{Eq. (1)}$$

where N_{eff} is cycle number until the electrode potential reached 0.5 V vs. Li^+/Li, Q_{cycle} is the electric charge for Li deposition/dissolution (0.2 C cm^{-2}), and Q_{ex} is the extra amount of electricity theoretically not necessary (0.8 C cm^{-2}). Aluminum corrosion was tested using a potential-step method with a Li/Al two-electrode coin-cell (2032 type) setup.

Single-crystal X-ray diffraction. Single-crystal X-ray diffraction measurements were performed using a R-axis Rapid II diffractometer (Rigaku Corporation) controlled by RAPID AUTO 2.40 software.[45] Crystals of $Li[C_2C_1im][FSA]_2$ were grown from the dichloromethane solution ($Li[C_2C_1im][FSA]_2$:dichloromethane = 10:1 in volume ($Li[C_2C_1im][FSA]_2$ melts just above room temperature)) by slowly cooling from 298 K to 243 K at a rate of 2.3 K h^{-1}. A selected crystal was then fixed on a quartz pin with pefluoropolyether oil under a dry air atmosphere and mounted on the diffractometer under a cold dry-nitrogen flow. Data collection was performed at 113 K and consisted of 12 ω scans (130–190°, 5° per frame) at fixed φ (0°) and χ (45°) angles and 32 ω scans (0–160°, 5° per frame) at fixed φ (180°) and χ (45°) angles. The X-ray output was 50 kV–40 mA and the exposure time was 400 s deg^{-1}. Integration, scaling, and absorption corrections were performed using RAPID AUTO 2.40 software. The structure was solved using SIR-92[46] and refined by SHELXL-97[47] linked to Win-

GX[48]. Anisotropic displacement factors were introduced for non-hydrogen atoms and hydrogen atoms were treated using an appropriate riding model.

Results and discussion

Thermal transitions. Figure 1 shows DSC curves at x(Li[FSA]) = 0.3, 0.5, and 0.8 and a summary of the DSC analysis for the Li[FSA]–[C_2C_1im][FSA] system. Table 1 lists the corresponding DSC data (see Figures S1−S9, Supporting Information).

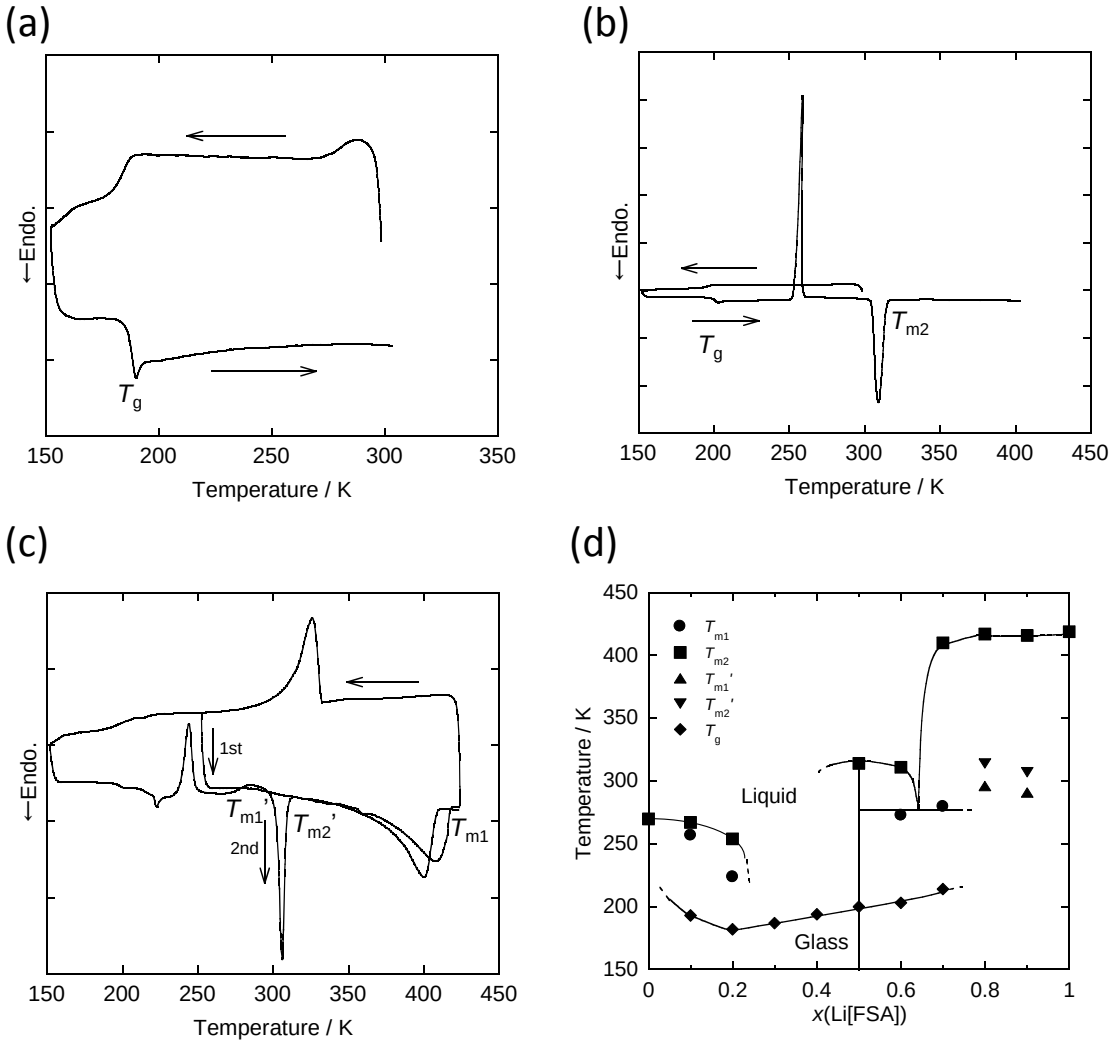

Figure 1 Differential scanning calorimetric curves at x(Li[FSA]) = (a) 0.3, (b) 0.5, and (c) 0.8 and (d) the resultant phase diagram for the Li[FSA]–[C_3C_1pyrr][FSA] system (see Supporting Information for the DSC curves at the other Li[FSA] fractions). T_{m1}: the onset temperature of melting, T_{m2}: the end temperature of melting, T_{m1}': the onset temperature of melting for the metastable phase, T_{m2}': the end temperature of melting for the metastable phase, and T_g: glass transition temperature.

Table 1 DSC transition temperatures for the Li[FSA]–[C_2C_1im][FSA] binary system. Enthalpy changes (/ kJ mol^{-1}) for the transition are given in parentheses

x(Li[FSA])	T_{m1} / K	T_{m2} / K	T_{m1}' / K	T_{m2}' / K	T_g / K
0.0	260 (9.3)	270	n.d.	n.d.	n.d.
0.1	257 (8.9)	267	n.d.	n.d.	193
0.2	224 (2.8)	254	n.d.	n.d.	182
0.3	n.d.	n.d.	n.d.	n.d.	187
0.4	n.d.	n.d.	n.d.	n.d.	194
0.5	305 (11)	314	n.d.	n.d.	200
0.6	273 (8.4)	311	n.d.	n.d.	203
0.7	280 (2.9)	410	n.d.	n.d.	214
0.8	n.d. (5.5)	417	296	314	n.d.
0.9	n.d. (7.2)	416	291	307	n.d.
1.0	413 (11)	419	n.d.	n.d.	n.d.

[a] T_{m1}: the onset temperature of melting, T_{m2}: the end temperature of melting, T_{m1}': the onset temperature of melting for the metastable phase, T_{m2}': the end temperature of melting for the metastable phase, T_g: glass transition temperature, and n.d.: not detected.

A wide liquid-phase temperature range around room temperature was observed between $0 \leq x$(Li[FSA]) ≤ 0.4. The supercooled ionic liquid formed the glass state at x(Li[FSA]) = 0.1, 0.2, 0.5, 0.6, and 0.7. The DSC analysis indicated that no crystallization occurred when x(Li[FSA]) = 0.3 and 0.4, which is the so-called crystallinity gap, and only the glass transition was observed (Figure 1 (a)). Although it is hard to predicate that these compositions thermodynamically do not form the crystalline state, there was no sign of crystallization even after refrigeration at 255 K for four weeks. The glass-transition temperature increases with increasing x(Li[FSA]), suggesting a low ion mobility at high Li[FSA] concentrations in the liquid state. During the heating scan from the supercooled state, the DSC curve for x(Li[FSA]) = 0.5 exhibited a sharp crystallization peak followed by a melting peak (Figure 1 (b)), indicating the existence of the 1:1 line compound Li[C_2C_1im][FSA]$_2$ (see below for the crystal structure of this compound). Several kinds of line compounds have previously been reported for some lithium sulfonylamide systems. In the Li[TFSA]-[$C_nC_1$im][TFSA] ($C_nC_1im^+$ = 1-alkyl-3-methylimidazolium) system, the 1:1 phase was observed for $C_1C_1im^+$ but not for $C_2C_1im^+$ and $C_4C_1im^+$ (namely, Li[C_1C_1im][TFSA]$_2$).[39] Instead, the Li[TFSA]-[C_2C_1im][TFSA] system possesses a 2:1 phase

($Li_2[C_2C_1im][TFSA]_3$).[49] During the heating scan, crystallization and melting of a metastable phase was observed when x(Li[FSA]) = 0.8 and 0.9 (Figure 1 (c)). Such metastable phases have not been reported not for the imidazolium-based Na analogue Na[FSA]-$[C_2C_1im][FSA]$,[50] but have been reported for the pyrrolidinium-based Na analogue Na[FSA]-$[C_3C_1pyrr][FSA]$.[51] The end temperatures of melting for these metastable phases (T_{m2}' = 314 K for x(Li[FSA]) = 0.8 and 307 K for x(Li[FSA]) = 0.9) are close to that for x(Li[FSA]) = 0.5 (T_{m2} = 314 K), indicating that the metastable phases appear as the $Li[C_2C_1im][FSA]_2$ double salt and melt to produce the thermodynamically stable state.

X-ray crystal structure of $Li[C_2C_1im][FSA]_2$. The crystal structure of $Li[C_2C_1im][FSA]_2$, corresponding to the crystal phase at x(Li[FSA]) = 0.5 in Figure 1, was determined by single-crystal X-ray diffraction measurements (see Table S1 for crystallographic data and refinement results). The disordering mode of $C_2C_1im^+$, coordination environment of Li^+, and packing diagram for this compound are summarized in Figure 2. The asymmetric unit contains a cation and anion pair (Figure S10), where $C_2C_1im^+$ is disordered in two positions correlated with the crystallographic inversion center located between the imidazolium rings (Figure 2 (a)). The FSA^- anion in this compound adopts the *cis*-structure,[52-55] *i.e.* the two F atoms are on the same side relative to the plane defined by the S−N−S bonds (F−S···S−F torsion angle of −6.81(9)°). The O3 and F2 atoms in FSA^- have large and highly anisotropic displacement factors, which reflects their slight disordering in the lattice. A similar but more significant disordering mode was reported in Cs[FSA].[53] The Li^+ cation is octahedrally coordinated by six O atoms in FSA^- (Li···O distances range: 2.0717(12)−2.1717(13) Å; O···Li···O angle range: 86.03(5)−93.97(5)°) (Figure 2 (b)). Two FSA^- anions coordinate to Li^+ in a bidentate manner, while two other FSA^- anions coordinate in a monodentate manner and bridge two other Li^+ ions. The coordination number of six is not very common for Li^+ although some examples are known such as Li[FSA],[56] $[Li(H_2O)][TFSA]$,[57] and $Li[C_1C_1im][TFSA]_2$[58]. This is in contrast to the lower coordination number in the liquid state of this system, as estimated by Raman spectroscopy and computational chemistry studies.[52]

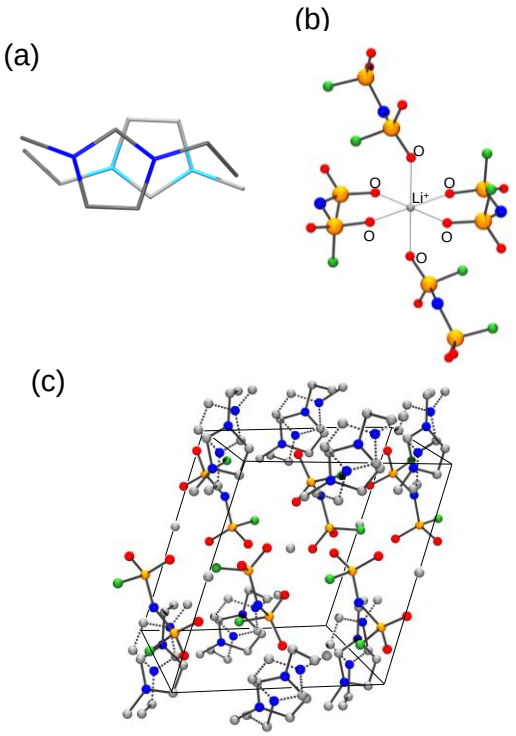

Figure 2 The X-ray crystal structure of $Li[C_2C_1im][FSA]_2$ determined at 113 K: (a) the disordering mode of $C_2C_1im^+$, (b) the coordination environment of Li^+ (Li···O distances: 2.0717(12)–2.1717(13) Å; O···Li···O angle: 86.03(5)–93.97(5)°), and (c) the packing diagram.

Comparison of the coordination states of Li^+ in Li[FSA] (6-coordinated),[56] $Li[C_2C_1im][FSA]_2$ (6-coordinated), Li[TFSA] (4-coordinated),[59] $Li_2[C_2C_1im][TFSA]_3$ (5-coordinated),[49] $Li[C_1C_1im][TFSA]_2$ (6-coordinated),[39] and $[Li(H_2O)][TFSA]$ (6-coordinated)[57] is made using the bond valence sum (BVS) method and the results are summarized in Table S2. The BVS method is a facile and quantitative way to evaluate the coordination state of an atom in a crystal lattice (see details in Supporting Information).[60-61] The BVS value for Li^+ in $Li[C_2C_1im][FSA]_2$ is 1.050, which is close to those for Li[FSA] (1.025, 1.081, and 1.081) and that for Li[TFSA] (1.050), suggesting that the octahedral coordination in $Li[C_2C_1im][FSA]_2$ is not an unusual coordination state. The Li^+ in $[Li(H_2O)][TFSA]$, with an average BVS of 0.978, is under-coordinated compared to the aforementioned cases. The BVS value of 1.142 for $Li_2[C_2C_1im][TFSA]_3$ is remarkable in this series, implying the over-coordination of Li^+ in this 5-coordinated state.

In the $Li[C_2C_1im][FSA]_2$ crystal lattice (Figure 2 (c)), the aforementioned Li^+ and FSA^- interaction leads to the formation of a 3D-network structure, with $C_2C_1im^+$ filling the space in the network by weakly interacting with the O atoms in FSA^- through C−H···O interactions. This packing mode may be called a layered structure but the boundary of the two layers (polar and apolar regions) is not clear compared with some other known TFSA salts such as $Li_2[C_2C_1im][TFSA]_3$. The $Li[C_1C_1im][TFSA]_2$ structure is also known to display a structure without a clear layered structure.

Physical properties. Figures 3, 4, and 5 show the temperature dependence of the density (ρ), viscosity (η), and ionic conductivity (σ), respectively, of the Li[FSA]–$[C_2C_1im][FSA]$ system and Tables 2, 3, and 4 list the corresponding data. The density of this system displays a linear dependence on temperature from 278 K to 358 K, which can be fitted by the following equation (Eq. (2)):

$$\rho = AT + B \qquad \text{Eq. (2)}$$

The A parameters (gradient) for Li[FSA]–$[C_2C_1im][FSA]$ are negative, suggesting that the density decreases with increasing temperature, and they tend to slightly decrease with increasing x(Li[FSA]). The B parameters (intercept) are positive and increase with increasing x(Li[FSA]), which implies that the addition of x(Li[FSA]) leads to the increase in density as differences in slope (A parameter) are not large. The molar concentration of the Li[FSA]–$[C_2C_1im][FSA]$ system was calculated at different x(Li[FSA]) values from the density and formula weight, as summarized in Table 5. The molar concentration at x(Li[FSA]) = 0.4 reaches 2.529 mol L^{-1} at 298 K and 2.428 mol L^{-1} at 358 K, which is advantageous for Li^+ transport in practical cells.

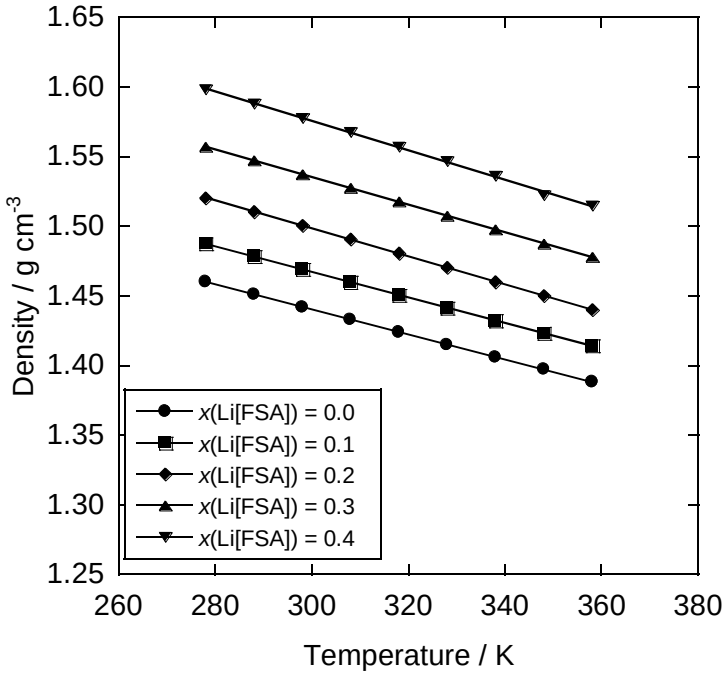

Figure 3 Density of the Li[FSA]–[C_2C_1im][FSA] ionic liquid for x(Li[FSA]) values of 0.0–0.4.

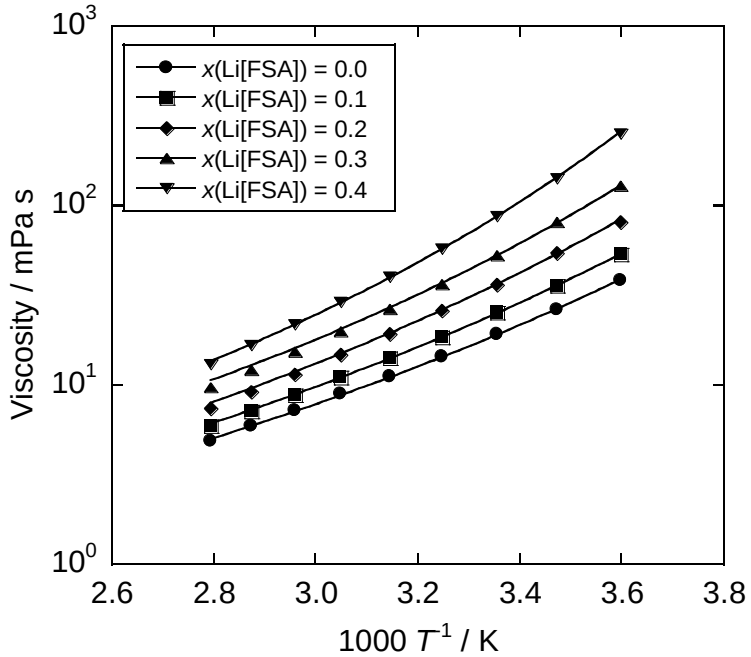

Figure 4 Arrhenius plots of the viscosity of the Li[FSA]–[C_2C_1im][FSA] ionic liquid for x(Li[FSA]) values of 0.0–0.4.

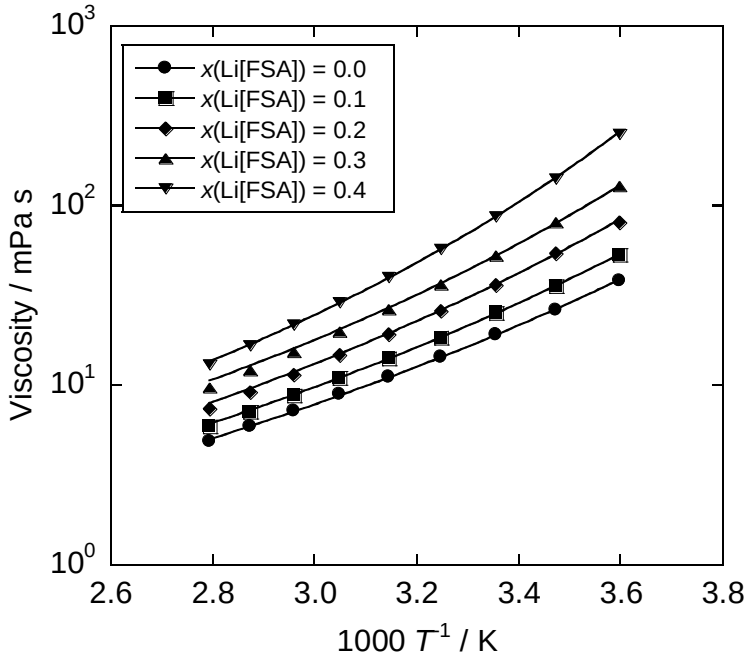

Figure 5. Arrhenius plots of the ionic conductivity of the Li[FSA]–[C_2C_1im][FSA] ionic liquid for *x*(Li[FSA]) values of 0.0–0.4.

Table 2 Density of the Li[FSA]–[C_2C_1im][FSA] ionic liquid

Temperature / K	Density / g cm^{-3} *x*(Li[FSA])				
	0.0	0.1	0.2	0.3	0.4
278	1.460	1.488	1.521	1.557	1.598
288	1.451	1.478	1.511	1.547	1.588
298	1.442	1.469	1.501	1.538	1.578
308	1.433	1.460	1.491	1.528	1.568
318	1.424	1.451	1.481	1.518	1.557
328	1.415	1.441	1.471	1.508	1.547
338	1.406	1.432	1.460	1.498	1.536
348	1.397	1.423	1.450	1.488	1.523
358	1.388	1.414	1.440	1.478	1.515
$A\times10^{4}$ [a]	−9.00	−9.19	−10.08	−9.94	−10.57
B [a]	1.71	1.74	1.80	1.83	1.89

[a] The symbols *A* and *B* are the constants in Eq. (2) for the temperature dependence of density.

Table 3 Viscosity of the Li[FSA]–[C_2C_1im][FSA] ionic liquid

Viscosity / mPa s					
Temperature / K	*x*(Li[FSA])				
	0.0	0.1	0.2	0.3	0.4
278	38.3	53.7	81.0	129.3	252.1
288	26.4	35.8	54.5	81.3	141.9
298	19.2	25.3	36.3	53.1	87.4
308	14.4	18.5	26.0	36.7	57.5
318	11.1	14.1	19.3	26.7	40.1
328	8.9	11.0	14.8	20.0	29.0
338	7.2	8.8	11.5	15.4	21.8
348	5.9	7.1	9.2	12.2	16.7
358	4.9	5.9	7.4	9.7	13.1

Table 4 Ionic conductivity of the Li[FSA]–[C_2C_1im][FSA] ionic liquid

Ionic conductivity / mS cm^{-1}					
Temperature / K	*x*(Li[FSA])				
	0.0	0.1	0.2	0.3	0.4
238	-	-	-	-	-
248	-	-	-	-	-
258	3.6	2.5	1.7	0.9	-
268	5.8	4.1	3.0	1.8	-
278	8.6	6.4	4.8	3.1	1.7
288	12.1	9.2	7.2	4.9	2.9
298	16.1	12.6	10.1	7.2	4.6
308	20.7	16.3	13.5	9.9	6.6
318	25.7	20.7	17.3	13.2	9.0
328	31.1	25.7	21.8	16.8	11.9
338	37.5	30.7	26.6	20.9	15.1
348	43.9	36.4	31.5	25.2	18.7
358	51.0	42.5	36.9	30.3	22.8
368	57.9	49.0	43.2	35.4	27.1
378	67.1	-	-	-	-
388	75.0	-	-	-	-

Table 5 Molar concentration of the Li[FSA]–[C_2C_1im][FSA] ionic liquid

Temperature / K	Molar concentration / mol L^{-1}			
	x(Li[FSA])			
	0.1	0.2	0.3	0.4
278	0.530	1.125	1.796	2.561
288	0.526	1.117	1.785	2.545
298	0.523	1.110	1.774	2.529
308	0.520	1.103	1.763	2.513
318	0.517	1.095	1.751	2.495
328	0.513	1.088	1.740	2.479
338	0.510	1.080	1.728	2.461
348	0.507	1.072	1.717	2.441
358	0.503	1.065	1.705	2.428

The viscosity and ionic conductivity of the Li[FSA]–[C_2C_1im][FSA] system do not exhibit Arrhenius-type temperature dependence. Instead, they are well-fitted by the Vogel-Tammann-Fulcher (VTF) equation[62-64] (Eqs. (3) and (4)):

$$\eta(T) = A_\eta \sqrt{T} \exp\left(\frac{B_\eta}{T - T_{0\eta}}\right) \quad \text{Eq. (3)}$$

$$\sigma(T) = \frac{A_\sigma}{\sqrt{T}} \exp\left(-\frac{B_\sigma}{T - T_{0\sigma}}\right) \quad \text{Eq. (4)}$$

The A_η, B_η, $T_{0\eta}$, A_σ, B_σ, and $T_{0\sigma}$ fitting parameters were determined by mathematical fitting (see Tables S3 and S4 for the fitting parameters ($R^2 > 0.99$)). Similar "fragile-liquid" behavior has also been reported for a range of other ionic liquids.[65-67] The ionic conductivity of neat [C_2C_1im][FSA] at 298 K was 16.1 mS cm^{-1}, which is close to previously reported values[12, 28, 51] and higher than that of neat [C_3C_1pyrr][FSA] (8.0 mS cm^{-1}). The ionic conductivity of 10.1 mS cm^{-1} at 298 K for x(Li[FSA]) = 0.2 (molar concentration of 1.110 mol L^{-1}) is reasonably high compared to those of nonaqueous electrolytes containing 1 M of Li salt used in Li secondary batteries. Although increasing x(Li[FSA]) results in decreased ionic conductivity owing to the viscosity increase, this drawback can be compensated by elevating the temperature, which enables the operation of ionic liquid electrolytes at high Li^+ contents.

For example, when x(Li[FSA]) = 0.2, heating enhances the ionic conductivity from 4.6 mS cm^{-1} at 298 K to 22.8 mS cm^{-1} at 368 K.

For many ionic liquids, molar ionic conductivity (λ), which is calculated from ionic conductivity and molar concentration, is correlated with viscosity as expressed by the Walden rule (Eq. (5)):[65, 68-73]

$$\lambda \cdot \eta = C \qquad \text{Eq. (5)}$$

where C is a constant. The Walden rule gives useful information on the dynamic properties of ionic liquids and is interpreted using the Walden plot of logarithmic molar conductivity versus logarithmic reciprocal viscosity. Figure 6 shows the Walden plot for the Li[FSA]–[C_2C_1im][FSA] system. Deviation of the gradient from unity requires modification of the Walden rule. In such cases, the fractional Walden rule can be introduced (Eq. (6)):

$$\lambda \cdot \eta^{\alpha} = C' \qquad \text{Eq. (6)}$$

where C' is another constant. The α parameter is the decoupling constant, which corresponds to the Walden-plot gradient and ranges from zero to one. The C' parameter corresponds to the Walden-plot intercept, and a small C' value means a shift of the plot to the bottom in the graph and occurs by greater association of the ions in an ionic liquid. The α parameters for the present Li[FSA]-[C_2C_1im][FSA] system are nearly constant (0.89 for x(Li[FSA]) = 0.0, 0.88 for x(Li[FSA]) = 0.1, 0.87 for x(Li[FSA]) = 0.2, 0.89 for x(Li[FSA]) = 0.3, and 0.89 for x(Li[FSA]) = 0.4) and close to or slightly smaller than the typical values for neat ionic liquids (0.90−0.95).[74-75] The C' parameter fluctuates slightly in this series (−0.13 for x(Li[FSA]) = 0.0, −0.15 for x(Li[FSA]) = 0.1, −0.13 for x(Li[FSA]) = 0.2, −0.17 for x(Li[FSA]) = 0.3, and −0.19 for x(Li[FSA]) = 0.4) but appears to generally decrease with increasing x(Li[FSA]). This trend can be reasonably explained by the introduction of Li^+, which is a small ion with

hard polarizability, causing the high degree of ion association observed for a certain x(Li[FSA]) range in the Li[FSA]-[C_3C_1pyrr][FSA] system.[37]

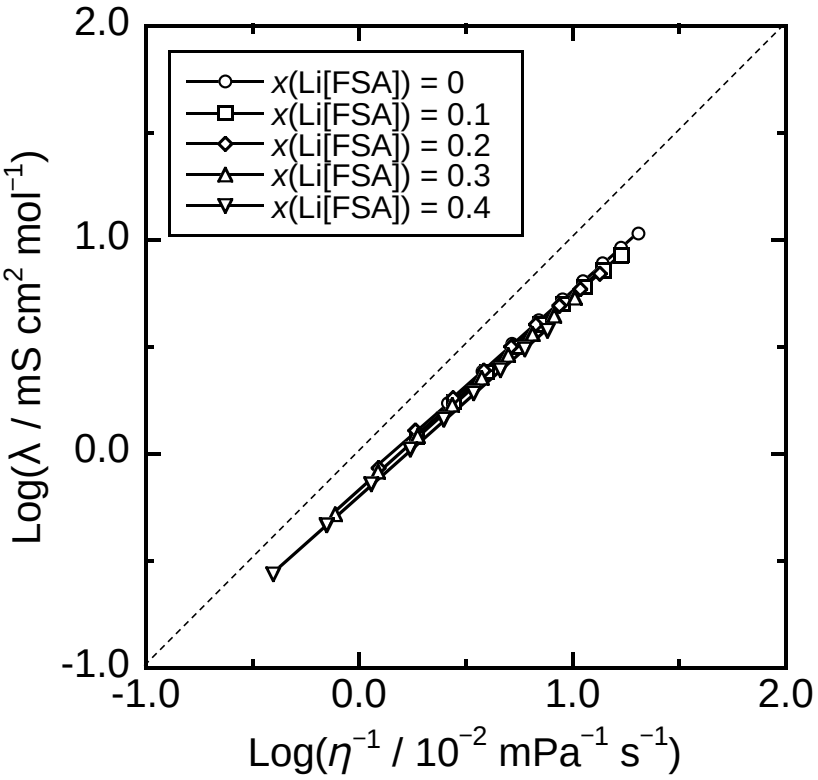

Figure 6 Walden plots for the Li[FSA]−[C_2C_1im][FSA] ionic liquids with x(Li[FSA]) values in the range of 0.0−0.4. The dashed line is a visual guide representing $\alpha = 1$ in the fractional Walden rule ($\lambda \cdot \eta^{\alpha} = C'$) as shown in Eq. (6).

Electrochemical stability. The electrochemical stability of the Li[FSA]-[C_2C_1im][FSA] ionic liquid was evaluated by cyclic voltammetry. Cyclic voltammograms of Cu disk (negative potential region), glass like carbon disk (positive potential region), and Al plate (positive potential region) electrodes in Li[FSA]-[C_2C_1im][FSA] (x(Li[FSA]) = 0.3) at 298 K are shown in Figure 7. In the negative potential region with the Cu electrode, Li metal deposition and dissolution were observed during the positive and negative scans, respectively, giving a Coulombic efficiency of 61%. Such stable Li metal deposition/dissolution has been observed in many FSA^--based ionic liquids, including Li[FSA]-

[C_2C_1im][FSA], Li[FSA]-[C_3C_1pyrr][FSA], and Li[FSA]-[C_4C_1pyrr][FSA].[12-18] The Al electrode does not exhibit any observable electrochemical activity below 5.0 V, which is attributed to the formation of a stable passivation film.

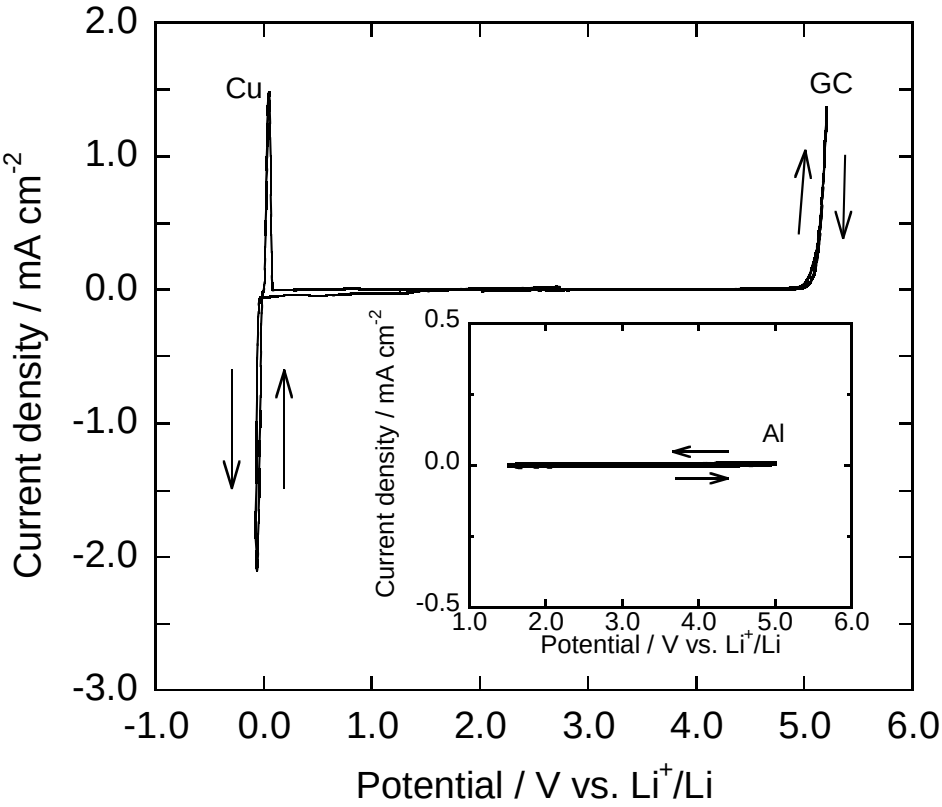

Figure 7 Cyclic voltammograms of Cu disk (negative potential region), glass like carbon disk (positive potential region), and Al plate (inset, positive potential region) electrodes in Li[FSA]–[C_2C_1im][FSA] (x(Li[FSA] = 0.3) at 298 K. Scan rate: 5 mV s^{-1}.

Cycle efficiency for lithium metal deposition/dissolution. The cycle efficiency for Li metal deposition/dissolution, ε_{cycle}, was evaluated according to Eq. (1). Voltage profiles during Li metal deposition/dissolution tests in the Li[FSA]-[C_2C_1im][FSA] ionic liquid (x(Li[FSA]) = 0.3) at 298, 333, and 363 K are shown in Figure 8. The temperature and x(Li[FSA]) dependences of the ε_{cycle} values are summarized in Figure 9 (see Figures S11−S19 for the voltage profiles when x(Li[FSA]) = 0.1, 0.2, and 0.4). The ε_{cycle} value for x(Li[FSA]) = 0.3 is 92% at 298 K and decreases with increasing temperature (82% at 333 K and 76% at 363 K). This trend is completely opposite to the case of Na metal in ionic

liquid electrolytes;[50, 76] the ε_{cycle} value of Na metal deposition/dissolution increases with increasing temperature (e.g. 69% at 298 K and 96% at 363 K for Na[FSA]-[C_2C_1im][FSA] (3:7) as determined by the same test). There are two possible factors that cause the decrease in ε_{cycle} for Li-metal deposition/dissolution: the reaction of Li metal with the ionic liquid (or with trace impurities) and the formation of dead Li metal. Elevated temperatures are thought to significantly enhance the reactivity of Li metal with ionic liquids, which is also related to the stability of the solid-electrolyte-interphase (SEI) layer. On the other hand, the formation of dead Li metal is caused by the dendritic deposition of Li metal, which is less suppressed for Li metal compared to Na metal in the present temperature range (333 and 363 K) because surface diffusion is enhanced near the melting point (the melting points of Li and Na metal are 454 and 371 K, respectively). Consequently, the reaction between Li metal and the ionic liquid contributes more significantly than the suppression of dead Li metal formation to the low ε_{cycle} values at elevated temperatures.

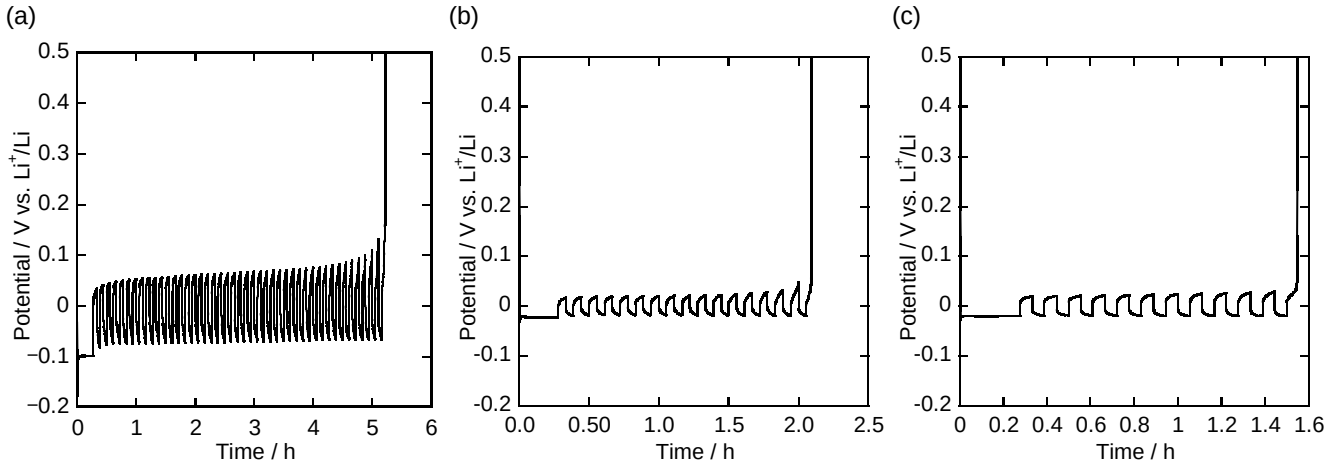

Figure 8 Voltage profiles during Li-metal deposition/dissolution in the Li[FSA]-[C_2C_1im][FSA] ionic liquid at (a) 298 K, (b) 333 K, and (c) 363 K at x(Na[FSA]) = 0.3. A Cu plate was used as the working electrode. Lithium metal of 0.8 C cm^{-2} was first deposited on the Cu substrate and Li deposition and dissolution of 0.2 C cm^{-2} were then repeated until the electrode potential reached 0.5 V vs. Li$^+$/Li during dissolution (see Experimental section for the details of these tests). The current density was 0.1 (or −0.1) mA cm^{-2} throughout these tests.

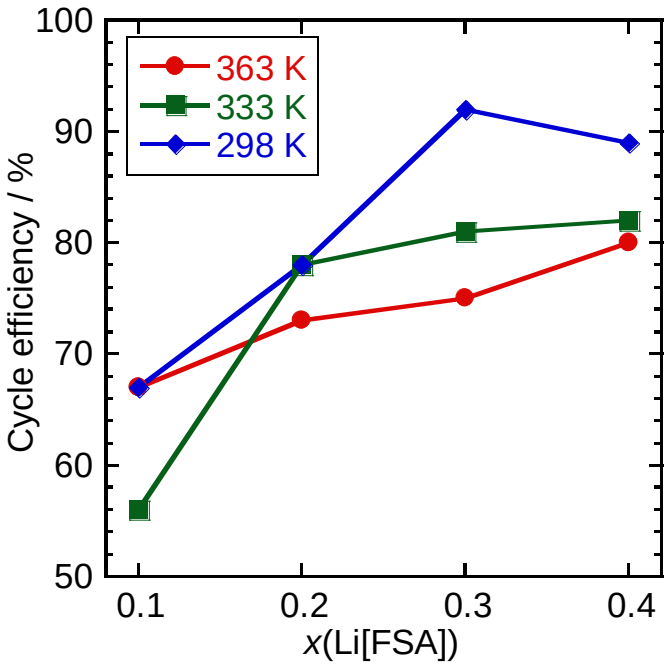

Figure 9 Cycle efficiency, ε_{cycle}, for Li metal deposition/dissolution in the Li[FSA]–[C_2C_1im][FSA] ionic liquid ($0.1 \leq x$(Li[FSA]) ≤ 0.4) at 298, 333, and 363 K.

Another trend found was that ε_{cycle} increases with increasing x(Li[FSA]), which is related to both of the two aforementioned factors. As reported previously, the Li^+ concentration affects the morphology of deposited Li metal, and Li metal deposited at higher Li^+ concentrations tends to be more dendritic.[77] Suppression of the reaction between the Li metal and ionic liquids is thought to occur at higher Li^+ concentrations since Li^+ is known to be an important component of the SEI layer and the formation of inorganic compounds facilitates SEI-layer stabilization.[19] The latter factor is considered to be more significant than the former factor in the present case, resulting in the high ε_{cycle} values at high x(Li[FSA]).

Aluminium corrosion behavior at positive potentials. The stability of Al electrodes at positive potentials is important when using Al as the current collector for positive electrodes. In addition to the cyclic voltammetric tests above, two kinds of potential-step tests were performed to further investigate Al stability in the Li[FSA]-[C_2C_1im][FSA] ionic liquid (x(Li[FSA]) = 0.3). Figure 10 shows the current-

density profile of an Al electrode when the potential was stepped from the rest potential to a certain positive potential (4.5, 4.6, 4.7, and 5.0 V vs. Li^+/Li). Figure 11 shows the current-density profile of an Al electrode when the potential was increased stepwise from 4.5 to 4.8 V by 0.05 V every 2 hours and then held at 4.8 V vs. Li^+/Li for 24 hours. Continuous oxidation of the Al electrode occurs above 4.6 V vs. Li^+/Li when directly stepping from the rest potential. Little current density was observed throughout the test when the potential was increased stepwise. These observations provide an important insight; the onset potential of Al corrosion depends on the method of polarization.

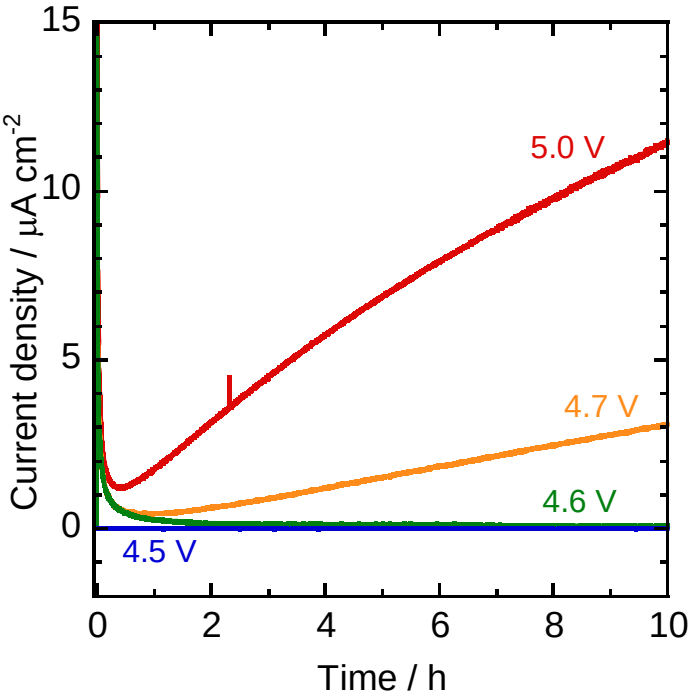

Figure 10 Current-density profiles for an Al plate electrode in Li[FSA]–[C_2C_1im][FSA] (x(Li[FSA]) = 0.3) at 298 K during potentiostatic electrolysis at 4.5, 4.6, 4.7, and 5.0 V vs. Li^+/Li.

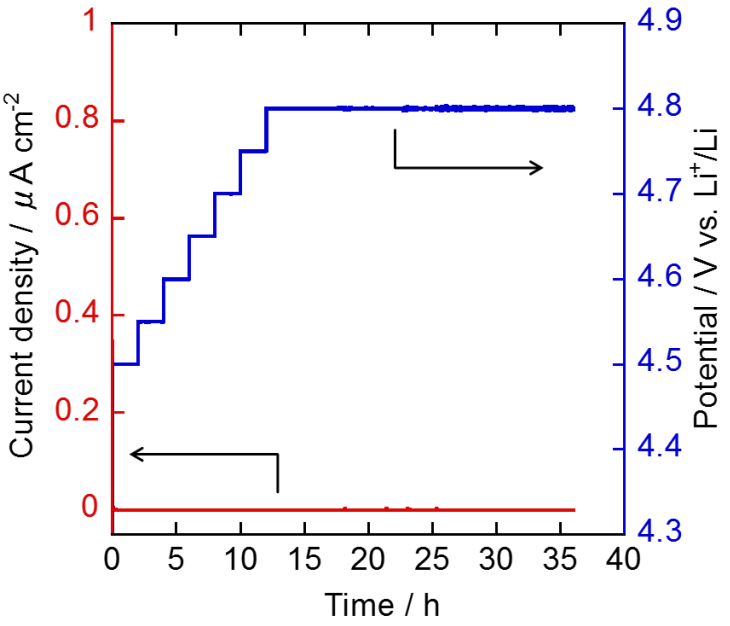

Figure 11 Potential dependence of current density for an Al plate electrode in Li[FSA]–[C_2C_1im][FSA] (x(Li[FSA] = 0.3) at 298 K. The potential was positively stepped from 4.5 V vs. Li^+/Li by 0.05 V every 2 hours and then held at 4.8 V vs. Li^+/Li for 24 hours.

Figure 12 shows the corrosion-limit potentials for an Al electrode in the Li[FSA]–[C_2C_1im][FSA] ionic liquid ($0.1 \leq x$(Li[FSA]) ≤ 0.4) at 298, 333, and 363 K. During this test, the potential was increased stepwise from 4.0 V or 4.5 V to 6.0 V vs. Li^+/Li by 0.1 V every 2 hours (see Figures S20−S31 for the current-density profile). The corrosion limit was defined as the potential at which the current density reached 0.5 μA cm^{-2}. The oxidative stability of the Al electrode is improved by increasing x(Li[FSA]) at 298 K, which suggests that the high Li^+ concentration leads to the formation of a stable passivation film. This may be explained by the low solubility of the surface film in the high-Li^+-content ionic liquid. At higher temperatures, this trend becomes less distinct and the Al electrode is corroded at relatively low potentials. This is likely due to the high solubility of the surface film in ionic liquid electrolytes at elevated temperatures. The Al metal stability in the present ionic liquid system is higher than that in organic solutions containing sulfonyl amide salts.[41, 78] This also agrees with the enhanced Al corrosion reported upon adding an organic solvent into ionic liquid electrolytes and the Al corrosion suppression reported upon adding an ionic liquid into organic electrolytic solutions. [79-80]

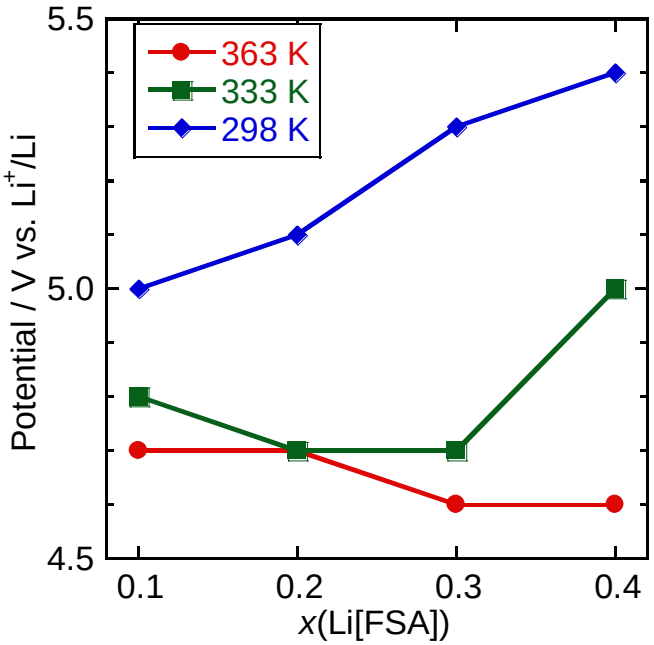

Figure 12 Corrosion-limit potential for an Al electrode in the Li[FSA]–[C_2C_1im][FSA] ionic liquid (x(Li[FSA]) range of 0.1−0.4) at 298, 333, and 363 K when the potential was increased stepwise from 4.0 V or 4.5 V to 6.0 V vs. Li^+/Li by 0.1 V every 2 hours (Figures S20−S31). The corrosion limit was defined as the potential at which the current density reached 0.5 μA cm^{-2}.

Figure 13 shows surface FE-SEM images of the Al electrode after anodic polarization in the Li[FSA]–[C_2C_1im][FSA] ionic liquid (x(Li[FSA]) = 0.4) at 363 K. The potential was increased stepwise (a) from 4.0 V to 4.3 V and (b) from 4.0 V to 6.0 V vs. Li^+/Li by 0.1 V every 2 hours (see Figures S32 and S33 for the corresponding EDX mapping images). When polarizing up to 4.3 V vs. Li^+/Li, island growths are observed on the Al surface (Region (B) in Figure 13) in addition to flat areas (Region (A) in Figure 13). Although C atoms were detected on the entire surface by EDX mapping, the islands contain more C atoms than the other areas. The islands do not contain Al and F atoms, but do contain S and O atoms. These EDX results suggest that the Al electrode was covered with a film formed by decomposition of the ionic liquid, which may also contain AlF_3 and Al_2O_3 (or related compounds), and that island growth of organic-based decomposition products occurs at certain points. On the other hand, the surface of the Al electrode polarized up to 6.0 V vs. Li^+/Li exhibits two distinct regions, neither of which contain significant amounts of C atoms. One region (Region D) is covered with a film composed

of O, F, and S atoms and a small amount of C atoms, suggesting a surface film originating from the ionic liquid still exists in this region. Only Al atoms are detected in Region C, indicating that the passivation film dissolved into the ionic liquid electrolyte and exposed bare Al metal upon polarization at 6.0 V vs. Li^+/Li.

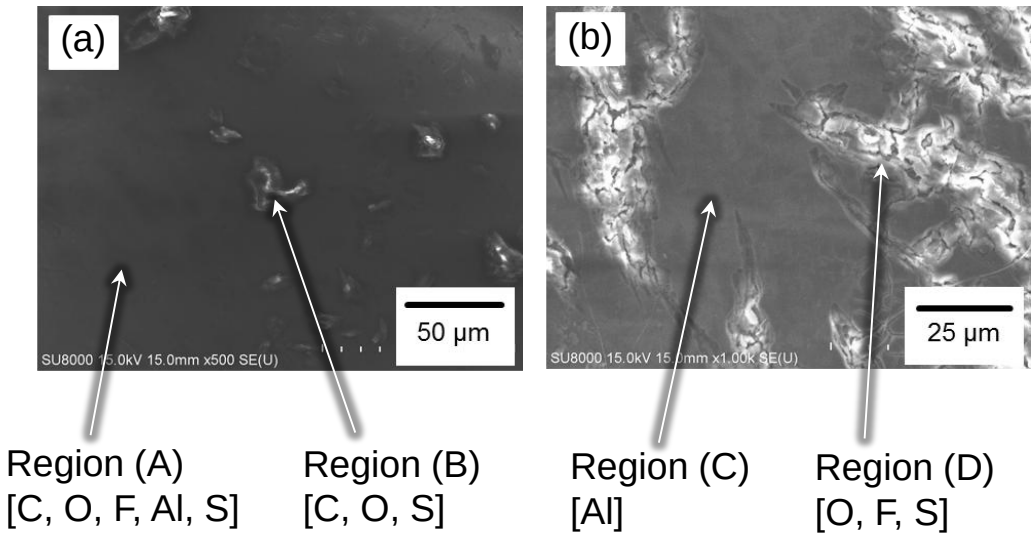

Figure 13 Surface FE-SEM images of an Al electrode after anodic polarization in the Li[FSA]–$[C_2C_1im][FSA]$ ionic liquid (x(Li[FSA]) = 0.4) at 363 K. The potential was increased stepwise (a) from 4.0 V to 4.3 V and (b) from 4.0 V to 6.0 V vs. Li^+/Li by 0.1 V every 2 hours. The main constituent atoms detected by EDX mapping are shown in square brackets. The corresponding EDX mapping images are shown in Figures S32 and S33.

Conclusions

We reported the thermal, physical, and electrochemical properties of $Li[N(SO_2F)_2]$-$[C_2C_1im][N(SO_2F)_2]$ ionic liquid electrolytes in view of their potential application in Li secondary batteries operating over wide temperature ranges. A phase diagram constructed from DSC measurements indicated that a wide liquid-phase temperature range exists between x(Li[FSA]) = 0.0–0.4, providing ionic liquid electrolytes with high Li^+ fractions (up to 2.529 mol L^{-1} at 298 K as Li[FSA]). The DSC measurements also indicated the existence of the $Li[C_2C_1im][FSA]_2$ line compound, corresponding to x(Li[FSA]) = 0.5. The crystal structure of $Li[C_2C_1im][FSA]_2$ contains Li^+ octahedrally coordinated by O atoms in FSA^- anion and disordered $C_2C_1im^+$ cations. The viscosity and ionic conductivity were fitted by the VTF

equation and are related by the fractional Walden rule. The electrochemical window is limited by Limetal deposition/dissolution at 0 V vs. Li^+/Li and oxidative decomposition of the ionic liquid around 5.1 V vs Li^+/Li. The Li metal deposition/dissolution cycle efficiency decreased with increasing temperature and decreasing x(Li[FSA]). The Al electrode stability also depended on temperature and x(Li[FSA]). High x(Li[FSA]) values also enhanced the stability but did not work effectively at elevated temperatures. This suggests that using an Al current collector in intermediate temperature ranges requires special attention, especially at high voltages. The experimental results presented here suggest that this ionic liquid system is highly useful as a safe electrolyte in Li secondary batteries either at room or elevated temperatures, while the optimal Li^+ concentration should be chosen carefully, depending on the purpose.

ASSOCIATED CONTENT

Supporting Information

Bond valence sum parameters, VTF fitting parameters, DSC curves, crystallographic data, and electrochemical data (Li deposition/dissolution cycle and Al corrosion tests). This material is available free of charge via the Internet at http://pubs.acs.org.

AUTHOR INFORMATION

Corresponding Author

*E-mail: k-matsumoto@energy.kyoto-u.ac.jp (Kazuhiko Matsumoto)

ACKNOWLEDTEMENTS

A part of this work was performed under a management of ‘Elements Strategy Initiative for Catalysts & Batteries (ESICB)’ supported by Ministry of Education, Culture, Sports, Science, and Technology,

Japan (MEXT).

Notes

The authors declare no competing financial interest.

REFERENCES

(1) Goodenough, J. B.; Park, K. S. The Li-Ion Rechargeable Battery: A Perspective. *J. Am. Chem. Soc.* **2013,** *135*, 1167-1176.
(2) Xu, K. Electrolytes and Interphases in Li-Ion Batteries and Beyond. *Chem. Rev.* **2014,** *114*, 11503-11618.
(3) Etacheri, V.; Marom, R.; Elazari, R.; Salitra, G.; Aurbach, D. Challenges in the Development of Advanced Li-Ion Batteries: A Review. *Energy Environ. Sci.* **2011,** *4*, 3243-3262.
(4) Ohno, H., *Electrochemical Aspects of Ionic Liquids*. 2nd ed.; John Wiley & Sons Inc.: Hoboken, New Jersey, 2011.
(5) Armand, M.; Endres, F.; MacFarlane, D. R.; Ohno, H.; Scrosati, B. Ionic-Liquid Materials for the Electrochemical Challenges of the Future. *Nature Mater.* **2009,** *8*, 621-629.
(6) MacFarlane, D. R.; Tachikawa, N.; Forsyth, M.; Pringle, J. M.; Howlett, P. C.; Elliott, G. D.; Davis, J. H.; Watanabe, M.; Simon, P.; Angell, C. A. Energy Applications of Ionic Liquids. *Energy Environ. Sci.* **2014,** *7*, 232-250.
(7) Lewandowski, A.; Swiderska-Mocek, A. Ionic Liquids as Electrolytes for Li-Ion Batteries-an Overview of Electrochemical Studies. *J. Power Sources* **2009,** *194*, 601-609.
(8) Welton, T. Room-Temperature Ionic Liquids. Solvents for Synthesis and Catalysis. *Chem. Rev.* **1999,** *99*, 2071-2083.
(9) Hallett, J. P.; Welton, T. Room-Temperature Ionic Liquids: Solvents for Synthesis and Catalysis. 2. *Chem. Rev.* **2011,** *111*, 3508-3576.
(10) Torimoto, T.; Tsuda, T.; Okazaki, K.; Kuwabata, S. New Frontiers in Materials Science Opened by Ionic Liquids. *Adv. Mater.* **2010,** *22*, 1196-1221.
(11) Zhang, H.; Feng, W. F.; Nie, J.; Zhou, Z. B. Recent Progresses on Electrolytes of Fluorosulfonimide Anions for Improving the Performances of Rechargeable Li and Li-Ion Battery. *J. Fluorine Chem.* **2015,** *174*, 49-61.
(12) Matsumoto, H.; Sakaebe, H.; Tatsumi, K.; Kikuta, M.; Ishiko, E.; Kono, M. Fast Cycling of Li/$LiCoO_2$ Cell with Low-Viscosity Ionic Liquids Based on Bis(fluorosulfonyl)imide $[FSI]^-$. *J. Power Sources* **2006,** *160*, 1308-1313.
(13) Basile, A.; Hollenkamp, A. F.; Bhatt, A. I.; O'Mullane, A. P. Extensive Charge-Discharge Cycling of Lithium Metal Electrodes Achieved Using Ionic Liquid Electrolytes. *Electrochem. Commun.* **2013,** *27*, 69-72.
(14) Best, A. S.; Bhatt, A. I.; Hollenkamp, A. F. Ionic Liquids with the Bis(fluorosulfonyl)imide Anion: Electrochemical Properties and Applications in Battery Technology. *J. Electrochem. Soc.* **2010,** *157*, A903-A911.
(15) Han, H. B.; Liu, K.; Feng, S. W.; Zhou, S. S.; Feng, W. F.; Nie, J.; Li, H.; Huang, X. J.; Matsumoto, H.; Armand, M., et al. Ionic Liquid Electrolytes Based on Multi-methoxyethyl Substituted Ammoniums and Perfluorinated Sulfonimides: Preparation, Characterization, and Properties. *Electrochim. Acta* **2010,** *55*, 7134-7144.

(16) Bhatt, A. I.; Best, A. S.; Huang, J. H.; Hollenkamp, A. F. Application of the N-Propyl-N-methyl-pyrrolidinium Bis(fluorosulfonyl)imide RTIL Containing Lithium Bis(fluorosulfonyl)imide in Ionic Liquid Based Lithium Batteries. *J. Electrochem. Soc.* **2010,** *157*, A66-A74.
(17) Paillard, E.; Zhou, Q.; Henderson, W. A.; Appetecchi, G. B.; Montanino, M.; Passerini, S. Electrochemical and Physicochemical Properties of $Py_{14}FSI$-Based Electrolytes with LiFSI. *J. Electrochem. Soc.* **2009,** *156*, A891-A895.
(18) Yoon, H.; Howlett, P. C.; Best, A. S.; Forsyth, M.; MacFarlane, D. R. Fast Charge/Discharge of Li Metal Batteries Using an Ionic Liquid Electrolyte. *J. Electrochem. Soc.* **2013,** *160*, A1629-A1637.
(19) Shkrob, I. A.; Marin, T. W.; Zhu, Y.; Abraham, D. P. Why Bis(fluorosulfonyl)imide Is a "Magic Anion" for Electrochemistry. *J. Phys. Chem. C* **2014,** *118*, 19661-19671.
(20) Seki, S.; Kobayashi, Y.; Miyashiro, H.; Ohno, Y.; Mita, Y.; Terada, N.; Charest, P.; Guerfi, A.; Zaghib, K. Compatibility of N-Methyl-N-propylpyrrolidinium Cation Room-Temperature Ionic Liquid Electrolytes and Graphite Electrodes. *J. Phys. Chem. C* **2008,** *112*, 16708-16713.
(21) Reiter, J.; Nadherna, M.; Dominko, R. Graphite and $LiCo_{1/3}Mn_{1/3}Ni_{1/3}O_2$ Electrodes with Piperidinium Ionic Liquid and Lithium Bis(fluorosulfonyl)imide for Li-Ion Batteries. *J. Power Sources* **2012,** *205*, 402-407.
(22) Saint, J.; Best, A. S.; Hollenkamp, A. F.; Kerr, J.; Shin, J. H.; Doeff, M. M. Compatibility of $Li_xTi_yMn_{1-y}O_2$ (y=0, 0.11) Electrode Materials with Pyrrolidinium-Based Ionic Liquid Electrolyte Systems. *J. Electrochem. Soc.* **2008,** *155*, A172-A180.
(23) Usui, H.; Masuda, T.; Sakaguchi, H. Li-Insertion/Extraction Properties of Si Thick-film Anodes in Ionic Liquid Electrolytes Based on Bis(fluorosulfonyl)amide and Bis(trifluoromethanesulfonyl)amide Anions. *Chem. Lett.* **2012,** *41*, 521-522.
(24) Usui, H.; Shimizu, M.; Sakaguchi, H. Applicability of Ionic Liquid Electrolytes to $LaSi_2$/Si Composite Thick-film Anodes in Li-Ion Battery. *J. Power Sources* **2013,** *235*, 29-35.
(25) Matsui, Y.; Kawaguchi, S.; Sugimoto, T.; Kikuta, M.; Higashizaki, T.; Kono, M.; Yamagata, M.; Ishikawa, M. Charge-discharge Characteristics of a $LiNi_{1/3}Mn_{1/3}Co_{1/3}O_2$ Cathode in FSI-Based Ionic Liquids. *Electrochemistry* **2012,** *80*, 808-811.
(26) Appetecchi, G. B.; Montanino, M.; Balducci, A.; Lux, S. F.; Winterb, M.; Passerini, S. Lithium Insertion in Graphite from Ternary Ionic Liquid-Lithium Salt Electrolytes I. Electrochemical Characterization of the Electrolytes. *J. Power Sources* **2009,** *192*, 599-605.
(27) Guerfi, A.; Duchesne, S.; Kobayashi, Y.; Vijh, A.; Zaghib, K. $LiFePO_4$ and Graphite Electrodes with Ionic Liquids Based on Bis(Fluorosulfonyl)Imide FSI^- for Li-Ion Batteries. *J. Power Sources* **2008,** *175*, 866-873.
(28) Ishikawa, M.; Sugimoto, T.; Kikuta, M.; Ishiko, E.; Kono, M. Pure Ionic Liquid Electrolytes Compatible with a Graphitized Carbon Negative Electrode in Rechargeable Lithium-ion Batteries. *J. Power Sources* **2006,** *162*, 658-662.
(29) Sugimoto, T.; Kikuta, M.; Ishiko, E.; Kono, M.; Ishikawa, M. Ionic Liquid Electrolytes Compatible with Graphitized Carbon Negative without Additive and Their Effects on Interfacial Properties. *J. Power Sources* **2008,** *183*, 436-440.
(30) Sugimoto, T.; Atsumi, Y.; Kono, M.; Kikuta, M.; Ishiko, E.; Yamagata, M.; Ishikawa, M. Application of Bis(fluorosulfonyl)imide-based Ionic Liquid Electrolyte to Silicon-nickel-carbon Composite Anode for Lithium-ion Batteries. *J. Power Sources* **2010,** *195*, 6153-6156.
(31) Matsui, Y.; Yamagata, M.; Murakami, S.; Saito, Y.; Higashizaki, T.; Ishiko, E.; Kono, M.; Ishikawa, M. Design of an Electrolyte Composition for Stable and Rapid Charging Discharging of a Graphite Negative Electrode in a Bis(fluorosulfonyl)imide-based Ionic Liquid. *J. Power Sources* **2015,** *279*, 766-773.
(32) Lewandowski, A. P.; Hollenkamp, A. F.; Donne, S. W.; Best, A. S. Cycling and Rate Performance of Li-$LiFePO_4$ Cells in Mixed FSI-TFSI Room Temperature Ionic Liquids. *J. Power Sources* **2010,** *195*, 2029-2035.

(33) Seki, S.; Takei, K.; Miyashiro, H.; Watanabe, M. Physicochemical and Electrochemical Properties of Glyme-LiN(SO_2F)$_2$ Complex for Safe Lithium-Ion Secondary Battery Electrolyte. *J. Electrochem. Soc.* **2011,** *158*.
(34) Zhou, Q.; Henderson, W. A.; Appetecchi, G. B.; Montanino, M.; Passerini, S. Physical and Electrochemical Properties of N-Alkyl-N-methylpyrrolidinium Bis(fluorosulfonyl)imide Ionic Liquids: Py_{13}FSI and Py_{14}FSI. *J. Phys. Chem. B* **2008,** *112*, 13577-13580.
(35) Tsunashima, K.; Kawabata, A.; Matsumiya, M.; Kodama, S.; Enomoto, R.; Sugiya, M.; Kunugi, Y. Low Viscous and Highly Conductive Phosphonium Ionic Liquids Based on Bis(fluorosulfonyl)amide Anion as Potential Electrolytes. *Electrochem. Commun.* **2011,** *13*, 178-181.
(36) Zhou, Q.; Henderson, W. A.; Appetecchi, G. B.; Passerini, S. Phase Behavior and Thermal Properties of Ternary Ionic Liquid-Lithium Salt (IL-IL-Li_x) Electrolytes. *J. Phys. Chem. C* **2010,** *114*, 6201-6204.
(37) Yoon, H.; Best, A. S.; Forsyth, M.; MacFarlane, D. R.; Howlett, P. C. Physical Properties of High Li-Ion Content N-Propyl-N-methylpyrrolidinium Bis(fluorosulfonyl)imide Based Ionic Liquid Electrolytes. *Phys. Chem. Chem. Phys.* **2015,** *17*, 4656-4663.
(38) Nadherna, M.; Reiter, J.; Moskon, J.; Dominko, R. Lithium Bis(fluorosulfonyl)imide-Pyr_{14}TFSI Ionic Liquid Electrolyte Compatible with Graphite. *J. Power Sources* **2011,** *196*, 7700-7706.
(39) Henderson, W. A.; Passerini, S. Phase Behavior of Ionic Liquid-Li_x Mixtures: Pyrrolidinium Cations and $TFSI^-$ Anions. *Chem. Mater.* **2004,** *16*, 2881-2885.
(40) Zhou, Q.; Boyle, P. D.; Malpezzi, L.; Mele, A.; Shin, J. H.; Passerini, S.; Henderson, W. A. Phase Behavior of Ionic Liquid-Li_x Mixtures: Pyrrolidinium Cations and $TFSI^-$ Anions - Linking Structure to Transport Properties. *Chem. Mater.* **2011,** *23*, 4331-4337.
(41) Abouimrane, A.; Ding, J.; Davidson, I. J. Liquid Electrolyte Based on Lithium Bis-fluorosulfonyl Imide Salt: Aluminum Corrosion Studies and Lithium Ion Battery Investigations. *J. Power Sources* **2009,** *189*, 693-696.
(42) Nohira, T.; Ishibashi, T.; Hagiwara, R. Properties of an Intermediate Temperature Ionic Liquid NaTFSA-CsTFSA and Charge-discharge Properties of $NaCrO_2$ Positive Electrode at 423 K for a Sodium Secondary Battery. *J. Power Sources* **2012,** *205*, 506-509.
(43) Chen, C. Y.; Matsumoto, K.; Nohira, T.; Ding, C. S.; Yamamoto, T.; Hagiwara, R. Charge-Discharge Behavior of a $Na_2FeP_2O_7$ Positive Electrode in an Ionic Liquid Electrolyte between 253 and 363 K. *Electrochim. Acta* **2014,** *133*, 583-588.
(44) Watarai, A.; Kubota, K.; Yamagata, M.; Goto, T.; Nohira, T.; Hagiwara, R.; Ui, K.; Kumagai, N. A Rechargeable Lithium Metal Battery Operating at Intermediate Temperatures Using Molten Alkali Bis(trifluoromethylsulfonyl)amide Mixture as an Electrolyte. *J. Power Sources* **2008,** *183*, 724-729.
(45) *Rapid Auto, Version 2.40*, Rigaku Corporation: Tokyo, Japan, 2006.
(46) Altomare, A.; Cascarano, G.; Giacovazzo, C.; Guagliardi, A. Completion and Refinement of Crystal-structures with SIR92. *J. Appl. Crystallogr.* **1993,** *26*, 343-350.
(47) Sheldrick, G. M. A Short History of Shelx. *Acta. Crystallogr. A* **2008,** *64*, 112-122.
(48) Farrugia, L. J. WinGX Suite for Small-molecule Single-crystal Crystallography. *J. Appl. Crystallogr.* **1999,** *32*, 837-838.
(49) Matsumoto, K.; Hagiwara, R.; Tamada, O. Coordination Environment around the Lithium Cation in Solid Li_2(EMIm)(N(SO_2CF_3)$_2$)$_3$ (EMIm=1-Ethyl-3-methylimidazolium): Structural Clue of Ionic Liquid Electrolytes for Lithium Batteries. *Solid State Sci.* **2006,** *8*, 1103-1107.
(50) Matsumoto, K.; Hosokawa, T.; Nohira, T.; Hagiwara, R.; Fukunaga, A.; Numata, K.; Itani, E.; Sakai, S.; Nitta, K.; Inazawa, S. The Na[FSA]-[C_2C_1im][FSA] ($C_2C_1im^+$:1-Ethyl-3-methylimidazolium and FSA^-:Bis(fluorosulfonyl)amide) Ionic Liquid Electrolytes for Sodium Secondary Batteries. *J. Power Sources* **2014,** *265*, 36-39.
(51) Matsumoto, K.; Okamoto, Y.; Nohira, T.; Hagiwara, R. Thermal and Transport Properties of Na[N(SO_2F)$_2$]-[N-Methyl-N-propylpyrrolidinium][N(SO_2F)$_2$] Ionic Liquids for Na Secondary Batteries. *J. Phys. Chem. C* **2015,** *119*, 7648-7655.

(52) Fujii, K.; Hamano, H.; Doi, H.; Song, X. D.; Tsuzuki, S.; Hayamizu, K.; Seki, S.; Kameda, Y.; Dokko, K.; Watanabe, M, et al. Unusual Li^+ Ion Solvation Structure in Bis(fluorosulfonyl)amide Based Ionic Liquid. *J. Phys. Chem. C* **2013,** *117*, 19314-19324.
(53) Matsumoto, K.; Oka, T.; Nohira, T.; Hagiwara, R. Polymorphism of Alkali Bis(Fluorosulfonyl)Amides ($M[N(SO_2F)_2]$, M = Na, K, and Cs). *Inorg. Chem.* **2013,** *52*, 568-576.
(54) Lopes, J. N. C.; Shimizu, K.; Padua, A. A. H.; Umebayashi, Y.; Fukuda, S.; Fujii, K.; Ishiguro, S. I. Potential Energy Landscape of Bis(fluorosulfonyl)amide. *J. Phys. Chem. B* **2008,** *112*, 9449-9455.
(55) Fujii, K.; Seki, S.; Fukuda, S.; Kanzaki, R.; Takamuku, T.; Umebayashi, Y.; Ishiguro, S. Anion Conformation of Low-viscosity Room-temperature Ionic Liquid 1-Ethyl-3-methylimidazolium Bis(fluorosulfonyl) Imide. *J. Phys. Chem. B* **2007,** *111*, 12829-12833.
(56) Beran, M.; Prihoda, J.; Zak, Z.; Cernik, M. A New Route to the Syntheses of Alkali Metal Bis(fluorosulfuryl)imides: Crystal Structure of $LiN(SO_2F)_2$. *Polyhedron* **2006,** *25*, 1292-1298.
(57) Xue, L. X.; Padgett, C. W.; DesMarteau, D. D.; Pennington, W. T. Synthesis and Structures of Alkali Metal Salts of Bis[(trifluoromethyl)sulfonyl]imide. *Solid State Sci.* **2002,** *4*, 1535-1545.
(58) Zhou, Q.; Fitzgerald, K.; Boyle, P. D.; Henderson, W. A. Phase Behavior and Crystalline Phases of Ionic Liquid-Lithium Salt Mixtures with 1-Alkyl-3-methylimidazolium Salts. *Chem. Mater.* **2010,** *22*, 1203-1208.
(59) Henderson, W. A.; Seo, D. M.; Zhou, Q.; Boyle, P. D.; Shin, J. H.; De Long, H. C.; Trulove, P. C.; Passerini, S. An Alternative Ionic Conductivity Mechanism for Plastic Crystalline Salt-Lithium Salt Electrolyte Mixtures. *Adv. Energy. Mater.* **2012,** *2*, 1343-1350.
(60) Brown, I. D.; Altermatt, D. Bond-valence Parameters Obtained from a Systematic Analysis of the Inorganic Crystal-structure Database. *Acta Crystallogr. B* **1985,** *41*, 244-247.
(61) Brese, N. E.; Okeeffe, M. Bond-valence Parameters for Solids. *Acta Crystallogr. B* **1991,** *47*, 192-197.
(62) Vogel, H. The Temperature Dependence Law of the Viscosity of Fluids. *Phys. Z.* **1921,** *22*, 645-646.
(63) Tammann, G.; Hesse, W. The Dependancy of Viscosity on Temperature in Hypothermic Liquids. *Z. Anorg. Allg. Chem.* **1926,** *156*.
(64) Fulcher, G. S. Analysis of Recent Measurements of the Viscosity of Glasses. *J. Am. Ceram. Soc.* **1925,** *8*, 339-355.
(65) Xu, W.; Cooper, E. I.; Angell, C. A. Ionic Liquids: Ion Mobilities, Glass Temperatures, and Fragilities. *J. Phys. Chem. B* **2003,** *107*, 6170-6178.
(66) Tokuda, H.; Hayamizu, K.; Ishii, K.; Abu Bin Hasan Susan, M.; Watanabe, M. Physicochemical Properties and Structures of Room Temperature Ionic Liquids. 1. Variation of Anionic Species. *J. Phys. Chem. B* **2004,** *108*, 16593-16600.
(67) Noda, A.; Hayamizu, K.; Watanabe, M. Pulsed-Gradient Spin-Echo H^1 and F^{19} NMR Ionic Diffusion Coefficient, Viscosity, and Ionic Conductivity of Non-chloroaluminate Room-temperature Ionic Liquids. *J. Phys. Chem. B* **2001,** *105*, 4603–4610.
(68) Walden, P.; Ulich, H.; Busch, G. Conductivity Measurements in Acetone. *Z. Phys. Chem.* **1926,** *123*, 429-434.
(69) Hagiwara, R.; Matsumoto, K.; Nakamori, Y.; Tsuda, T.; Ito, Y.; Matsumoto, H.; Momota, K. Physicochemical Properties of 1,3-Dialkylimidazolium Fluorohydrogenate Room-temperature Molten Salts. *J. Electrochem. Soc.* **2003,** *150*, D195-D199.
(70) Yoshida, Y.; Muroi, K.; Otsuka, A.; Saito, G.; Takahashi, M.; Yoko, T. 1-Ethyl-3-methylimidazolium Based Ionic Liquids Containing Cyano Groups: Synthesis, Characterization, and Crystal Structure. *Inorg. Chem.* **2004,** *43*, 1458-1462.
(71) Xu, W.; Angell, C. A. Solvent-free Electrolytes with Aqueous Solution - Like Conductivities. *Science* **2003,** *302*, 422-425.
(72) MacFarlane, D. R.; Forsyth, M.; Izgorodina, E. I.; Abbott, A. P.; Annat, G.; Fraser, K. On the Concept of Ionicity in Ionic Liquids. *Phys. Chem. Chem. Phys.* **2009,** *11*, 4962-4967.

(73) Yoshizawa, M.; Xu, W.; Angell, C. A. Ionic Liquids by Proton Transfer: Vapor Pressure, Conductivity, and the Relevance of ΔpK_a from Aqueous Solutions. *J. Am. Chem. Soc.* **2003,** *125*.
(74) Schreiner, C.; Zugmann, S.; Hartl, R.; Gores, H. J. Fractional Walden Rule for Ionic Liquids: Examples from Recent Measurements and a Critique of the So-called Ideal KCl Line for the Walden Plot. *J. Chem. Eng. Data* **2010,** *55*, 1784-1788.
(75) Harris, K. R. Relations between the Fractional Stokes-Einstein and Nernst-Einstein Equations and Velocity Correlation Coefficients in Ionic Liquids and Molten Salts. *J. Phys. Chem. B* **2010,** *114*, 9572-9577.
(76) Matsumoto, K.; Taniki, R.; Nohira, T.; Hagiwara, R. Inorganic-organic Hybrid Ionic Liquid Electrolytes for Na Secondary Batteries. *J. Electrochem. Soc.* **2015,** *162*, A1409-A1414.
(77) Nishida, T.; Nishikawa, K.; Rosso, M.; Fukunaka, Y. Optical Observation of Li Dendrite Growth in Ionic Liquid. *Electrochim. Acta* **2013,** *100*, 333-341.
(78) Han, H. B.; Zhou, S. S.; Zhang, D. J.; Feng, S. W.; Li, L. F.; Liu, K.; Feng, W. F.; Nie, J.; Li, H.; Huang, X. J., et al. Lithium Bis(Fluorosulfonyl)Imide (LiFSI) as Conducting Salt for Nonaqueous Liquid Electrolytes for Lithium-ion Batteries: Physicochemical and Electrochemical Properties. *J. Power Sources* **2011,** *196*, 3623-3632.
(79) Evans, T.; Olson, J.; Bhat, V.; Lee, S. H. Effect of Organic Solvent Addition to $Pyr_{13}FSI$ + LiFSI Electrolytes on Aluminum Oxidation and Rate Performance of $Li(Ni_{1/3}Mn_{1/3}Co_{1/3})O_2$ Cathodes. *J. Power Sources* **2014,** *265*, 132-139.
(80) Hofmann, A.; Merklein, L.; Schulz, M.; Hanemann, T. Anodic Aluminum Dissolution of LiTFSA Containing Electrolytes for Li-ion-batteries. *Electrochim. Acta* **2014,** *116*, 388-395.